WILEY-VCH

d by

ıtxu Lanceros-Méndez and Pedro Martins

ıgnetoelectric lymer-Based mposites

amentals and Applications

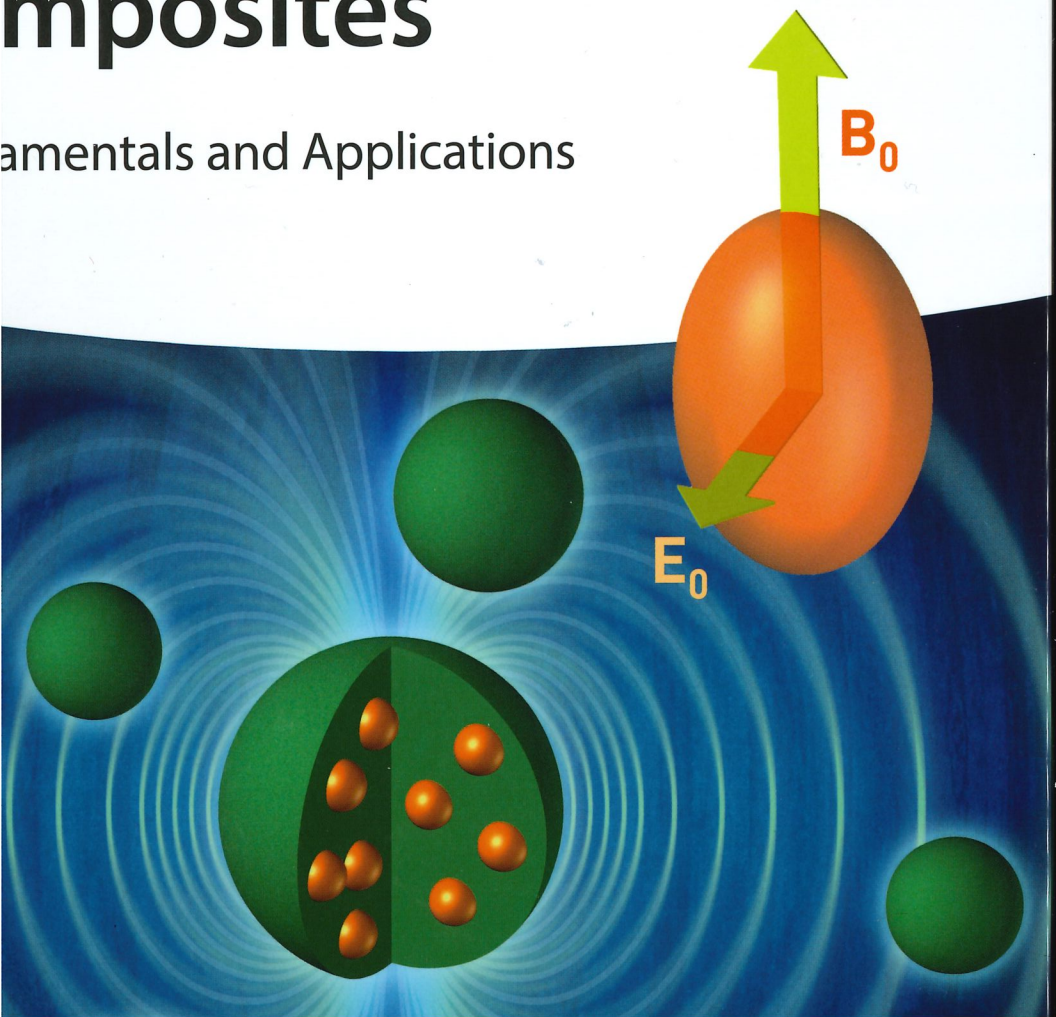

Magnetoelectric Polymer-Based Composites

Fundamentals and Applications

Edited by Senentxu Lanceros-Méndez and Pedro Martins

WILEY-VCH

Editors

Prof. Senentxu Lanceros-Méndez
Universidade do Minho
Centro de Física
Campus de Gualtar
Braga 4710-057
Portugal

Prof. Pedro Martins
Universidade do Minho
Centro de Física
Campus de Gualtar
Braga 4710-057
Portugal

All books published by **Wiley-VCH** are carefully produced. Nevertheless, authors, editors, and publisher do not warrant the information contained in these books, including this book, to be free of errors. Readers are advised to keep in mind that statements, data, illustrations, procedural details or other items may inadvertently be inaccurate.

Library of Congress Card No.: applied for

British Library Cataloguing-in-Publication Data
A catalogue record for this book is available from the British Library.

Bibliographic information published by the Deutsche Nationalbibliothek
The Deutsche Nationalbibliothek lists this publication in the Deutsche Nationalbibliografie; detailed bibliographic data are available on the Internet at <http://dnb.d-nb.de>.

© 2017 Wiley-VCH Verlag GmbH & Co. KGaA, Boschstr. 12, 69469 Weinheim, Germany

All rights reserved (including those of translation into other languages). No part of this book may be reproduced in any form – by photoprinting, microfilm, or any other means – nor transmitted or translated into a machine language without written permission from the publishers. Registered names, trademarks, etc. used in this book, even when not specifically marked as such, are not to be considered unprotected by law.

Print ISBN: 978-3-527-34127-6
ePDF ISBN: 978-3-527-80134-3
ePub ISBN: 978-3-527-80135-0
Mobi ISBN: 978-3-527-80136-7
oBook ISBN: 978-3-527-80133-6

Cover Design Schulz Grafik-Design, Fußgönheim, Germany
Typesetting SPi Global, Chennai, India
Printing and Binding Markono Print Media Pte Ltd, Singapore

Printed on acid-free paper

Alex Alexei Volinsky
University of South Florid
College of Engineering
Department of Mechanical Engineering
Tampa, FL 33620
USA

Gordon G. Wallace
University of Wollongong
ARC Centre of Excellence for Electromaterials Science
Intelligent Polymer Research Institute/AIIM Faculty
Innovation Campus, Squires Way
NSW 2522
Australia

Chengzhou Xin
Tsinghua University
School of Materials Science and Engineering, and State Key Lab of New Ceramics and Fine Processing
Beijing 100084
China

Zhilian Yue
University of Wollongong
ARC Centre of Excellence for Electromaterials Science
Intelligent Polymer Research Institute/AIIM Faculty
Innovation Campus, Squires Way
NSW 2522
Australia

Jia-Wei Zhang
Northeast Electric Power University
School of Electrical Engineering
169 Changchun Road
Jilin 132013
China

and

Harbin University of Science and Technology Key Laboratory of Engineering Dielectric and its Application of Ministry of Education
Harbin
China

Tian Zheng
University of Wollongong
ARC Centre of Excellence for Electromaterials Science
Intelligent Polymer Research Institute/AIIM Faculty
Innovation Campus, Squires Way
NSW 2522
Australia

Yan Zong
University of Wollongong
ARC Centre of Excellence for Electromaterials Science
Intelligent Polymer Research Institute/AIIM Faculty
Innovation Campus, Squires Way
NSW 2522
Australia

Zhijun Zuo
Functional Materials Research Institute
Central Iron and Steel Research Institute
No. 76 Xueyuan South Road
Beijing 100081
China

3b

Polymer-Based Magnetoelectric Composites: Polymer as a Binder

Yang Song[1,2], *De'an Pan*[3], *Zhijun Zuo*[4], *and Alex Alexei Volinsky*[2]

[1] *University of Science and Technology Beijing, Department of Mechanical Engineering, Institute for Advanced Materials and Technology, 30 Xueyuan Road, Beijing, 100083, China*
[2] *University of South Florida, College of Engineering, Department of Mechanical Engineering, 4202 E Fowler Ave, Tampa, FL 33620, USA*
[3] *Beijing University of Technology, Institute of Circular Economy, 100 Ping Le Yuan, Beijing, 100124, China*
[4] *Functional Materials Research Institute, Central Iron and Steel Research Institute, No. 76 Xueyuan South Road, Beijing, 100081, China*

3b.1 Introduction

The magnetoelectric (ME) effect is defined as the induced dielectric polarization under applied magnetic field (H) through interfacial strain coupling of the two phases or as the induced magnetization in the presence of an applied electric field [1]. ME composites made by combining piezoelectric (PE) and piezomagnetic (PM) materials can lead to remarkable ME effects at room temperature, compared with the single-phase MEs [2–4]. Recently, ME composites have drawn much attention as a popular research topic because of excellent ME performance at room temperature for potential applications in multifunctional devices, such as memory devices, tunable microwave devices, and sensors [5–7].

Giant magnetostrictive material, Terfenol-D ($Tb_{1-x}Dy_xFe_{2-y}$), alloy is one of the best PM candidates for ME composites [8]. However, some Terfenol-D properties, including low mechanical strength, high eddy current losses at high working frequencies, and fabrication size limits, hinder ME composite applications [9]. To solve the aforementioned problems, polymer-bonded (based) ME composites are considered to have distinct advantages [10]. They are highly flexible, nonbrittle, and allow simple manufacturing processes at room temperature with various shapes and sizes. In this chapter, representative results of polymer-based (polymer as a binder) $Tb_{1-x}Dy_xFe_{2-y}$/Pb(Zr, Ti)O_3 ME composites are introduced to show how they are made and their structural design is improved. Single- and multi-electrode cylindrical ME composite are described. The effects of polymer content and particle size on the composites are discussed. All studies utilized $Tb_{1-x}Dy_xFe_{2-y}$(Terfenol-D) and Pb(Zr, Ti)O_3 (PZT) as the PM and PE phases, respectively.

Magnetoelectric Polymer-Based Composites: Fundamentals and Applications, First Edition.
Edited by Senentxu Lanceros-Méndez and Pedro Martins.
© 2017 Wiley-VCH Verlag GmbH & Co. KGaA. Published 2017 by Wiley-VCH Verlag GmbH & Co. KGaA.

3b.2 Polymer-Based $Tb_{1-x}Dy_xFe_{2-y}$ by Magnetic Warm Compaction

The research described in this chapter developed from previous experiments on the enhanced ME effect in magnetostrictive/piezoelectric laminates by adopting magnetic warm compaction Terfenol-D [11]. In recent years, various ME composites have been developed, including $Tb_{0.27-x}Dy_{0.73-y}Y_{x+y}Fe_2$/PVDF composites, $(x)CoFe_2O_4$-$(1-x)Pb_{0.7}Ca_{0.3}TiO_3$ composites, and $(Tb_{0.3}Dy_{0.7})_{0.75}Pr_{0.25}Fe_{1.55}$-$Pb(Zr_{0.53}Ti_{0.47})O_3$ nano-ceramic composites. Among them, layered ME composites with different structures exhibit enhanced ME effects due to mechanical coupling between piezoelectric and magnetostrictive layers. Giant magnetostrictive material $Tb_{1-x}Dy_xFe_{2-y}$ was combined with piezoelectric materials to obtain higher ME voltage coefficient, such as lead zirconium titanate (PZT) and polyvinylidene fluoride (PVDF). To avoid huge eddy current loss under high frequencies, the Terfenol-D component is generally made into a bonded magnet. In this chapter, ME composites laminated with the bonded Terfenol-D prepared by magnetic warm compaction and PZT ceramics were fabricated, and the ME voltage coefficient of the composites was measured.

3b.2.1 Experiment for Magnetic Warm Compaction

The preparation process of the bilayered ME composites made up of the bonded Terfenol-D and sintered PZT bulk is illustrated in Figure 3b.1. As shown in Figure 3b.1a, the magnetic warm compaction includes magnetic field application, accompanied by heating and pressing. Directionally solidified Terfenol-D alloy was crushed into powder, with randomly distributed size <180 μm. A homogeneous mixture consisting of 97 wt% Terfenol-D powder and 3 wt% epoxy resin binder was prepared for the compaction process. The bulk density and softening transition temperature of the thermosetting epoxy resin were 1.1 g cm^{-3} and 100 °C, respectively. Three different types of bonded Terfenol-D samples were fabricated. Sample 1 was prepared under 154 MPa at room temperature. The process of preparing Samples 2 and 3 are as follows. The mixture of Terfenol-D powder and epoxy resin was filled into the mold preheated to 130 °C. After 20 s of heating, Sample 2 was obtained under 154 MPa. Similarly, Sample 3 was prepared under 154 MPa and 2 T oriented magnetic field along the length direction of the sample at 130 °C. The dimensions of the bonded Terfenol-D composites are $33 \times 10 \times 10$ mm^3, as shown in Figure 3b.1b. Commercial $(Pb(Zr_{0.52}Ti_{0.48})O_3$,

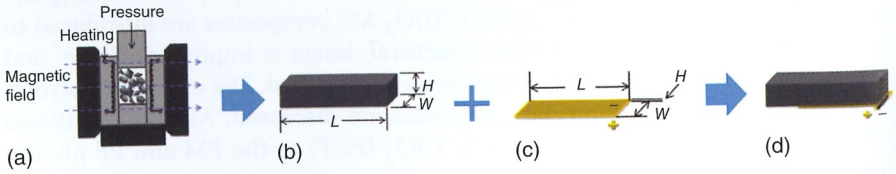

Figure 3b.1 Illustration of the preparation process and ME measurement of the bonded Terfenol-D/PZT bilayered ME composites: (a) warm compaction process; (b) Terfenol-D polymer compacted sample; (c) PZT plate; and (d) ME composite.

PZT-5H, ceramic with $25 \times 10 \times 1$ mm^{3}dimensions was used as the piezoelectric layer, as shown in Figure 3b.1c. The densities of the three samples were about 5.78, 6.91, and 6.95 g cm^{-3}, respectively. The bonded Terfenol-D and the PZT-5H were combined into a bonded Terfenol-D/PZT-5H bilayered ME composites with cyanoacrylate (super glue), as shown in Figure 3b.1d. The ME voltage coefficient was measured in the ME measurement system. The voltage δV across the sample was amplified and measured with an oscilloscope. The ME voltage coefficient was calculated based on $\alpha_E = \delta V/(t_{PZT}\,\delta H)$, where t_{PZT} is the thickness of PZT-5H and δH is the amplitude of ac magnetic field generated by Helmholtz coils. In the experiment, δH is 1.2 Oe when the ac current flowing through the coil is 1 A. This work focused on the transverse coefficient $\alpha_{E,31}$ of the three samples.

3b.2.2 Results and Discussion of Magnetic Warm Compaction

The frequency dependence of $\alpha_{E,31}$ was measured under the dc magnetic field of $H_{dc} = 1100$ kOe, as shown in Figure 3b.2. Three peaks appear for all the three samples when the applied ac magnetic field varied from 1 to 60 kHz. The largest ME coefficient is about 1.5, 2, and 6 V cm^{-1} Oe^{-1} for the three samples, respectively. The ME coefficient of Sample 3 was enhanced about thrice compared with Sample 1 and about twice compared with Sample 2. The corresponding peaks of the three samples appeared under different frequencies. It is reasonable to explain that the different peak frequencies are corresponding to the density and Young's modulus for different samples.

The ME voltage coefficient dependence on the applied magnetic field H_{dc} ranging from 0 to 5 kOe is shown in Figure 3b.3. It can be noted that the ME coefficient of Sample 1 is larger than the other samples when the ac magnetic field is applied at 1 kHz and f_{r2}. The largest ME coefficient is 6 V cm^{-1} Oe^{-1} at f_{r2} for Sample 3. The highest ME voltage coefficient is about 2 V cm^{-1} Oe^{-1} for Samples 1 and 2. It can be concluded from Figures 3b.2 and 3b.3 that magnetic warm compaction technique is an effective technology to enhance the ME voltage coefficient of the

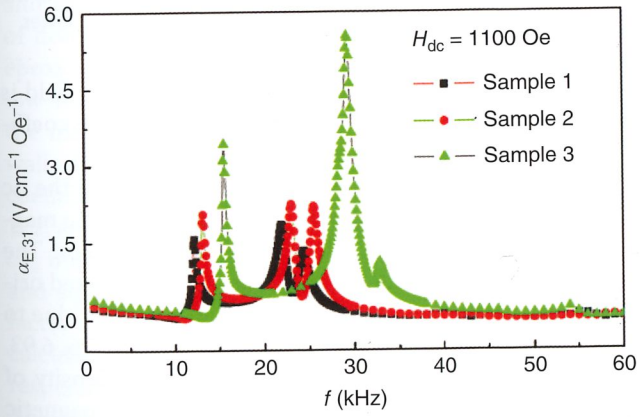

Figure 3b.2 Frequency dependence of $\alpha_{E,31}$ with $H_{dc} = 1100$ Oe. Zuo *et al.* 2014 [11]. Reproduced with permission of Elsevier.

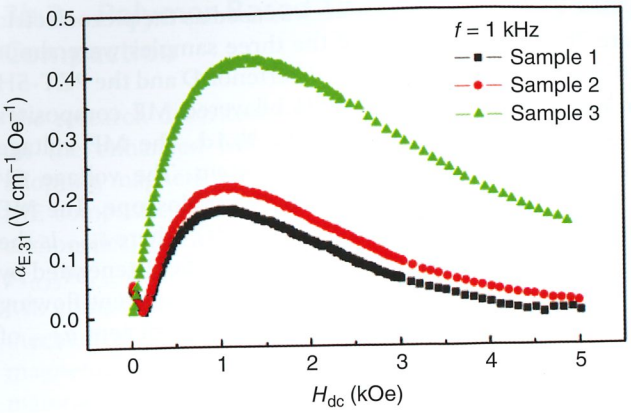

Figure 3b.3 The ME voltage coefficient dependence on the applied magnetic field H_{dc} ranging from 0 to 5 kOe. Zuo *et al.* 2014 [11]. Reproduced with permission of Elsevier.

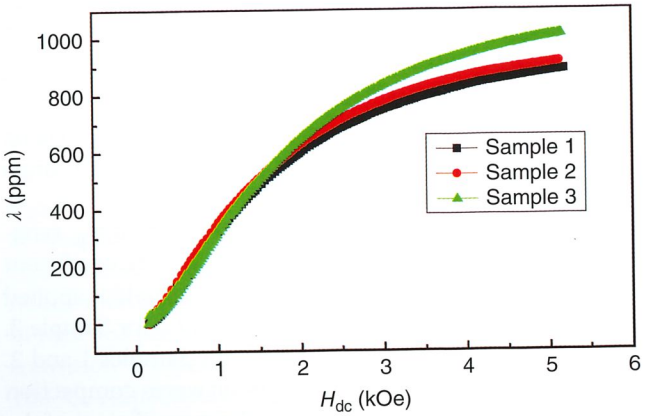

Figure 3b.4 Magnetostrictive coefficient dependence on the applied magnetic field H_{dc} of the bonded Terfenol-D composites. Zuo *et al.* 2014 [11]. Reproduced with permission of Elsevier.

bonded Terfenol-D/PZT composites. Additionally, optimizing magnetic field is more effective than the heating procedure for enhancing the ME voltage coefficient using the method of magnetic warm compaction.

Figure 3b.4 represents the magnetostrictive coefficient dependence of the dc magnetic field H_{dc} of the bonded Terfenol-D magnet. It is obvious that the magnetostrictive coefficient of Sample 3 is superior to that of other samples. The magnetostrictive coefficient depends on the density and degree of preferred orientation. The density of Samples 2 and 3 is greater than that of Sample 1 due to lower mixture viscosity at 130 °C. The bonded Terfenol-D density is 5.76, 6.93, and 6.95 g cm^{-3}, for Samples 1, 2, and 3, respectively. However, the density of Sample 3 is barely changed compared with Sample 2 when directional magnetic field is applied at 130 °C. Comparable ME voltage coefficients of Samples 1 and 2 are attributed to the enhanced density effects.

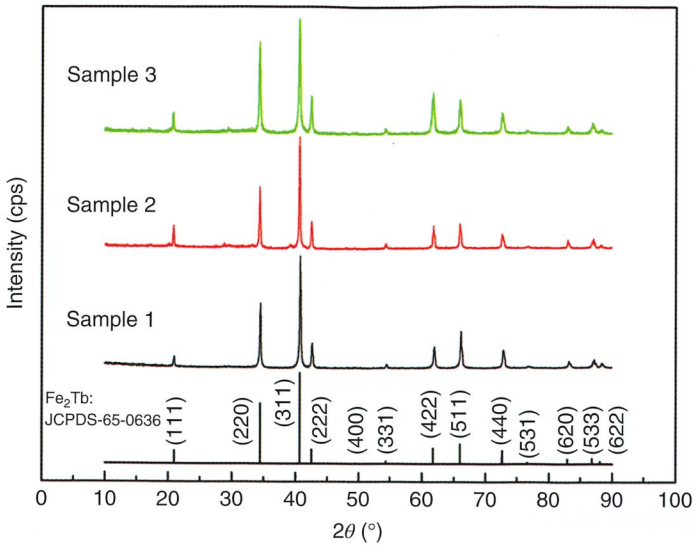

Figure 3b.5 XRD patterns of the bonded Terfenol-D composites. Zuo *et al.* 2014 [11]. Reproduced with permission of Elsevier.

Figure 3b.5 depicts XRD patterns of the bonded Terfenol-D magnets. The XRD pattern of Sample 1 is almost identical to the standard Terfenol-D X-ray diffraction (XRD) pattern. The relative intensities along the (111) and (422) reflections for Samples 2 and 3 are slightly higher than Sample 1. The relative intensities of the (220), (222), and (422) reflections of Sample 3 are stronger than Sample 2. Magnetostriction along the <220>, <222>, and <422> directions contributes more to the overall magnetostriction coefficient due to the relatively high magnetic anisotropy of Terfenol-D. The differences in XRD patterns can explain the magnetostriction results and reflect the orientation effect of the magnetic field. It is also noticed that the magnetostriction of Sample 3 is smaller than Samples 1 and 2 under low magnetic field but is larger under strong magnetic field. In terms of domain motion, the prestress applied to the Terfenol-D particles by cured epoxy matrix makes the non-180° domain walls more difficult to move under low magnetic field, resulting in a smaller magnetostriction coefficient. With the magnetic field increase, Sample 3, which exhibits more non-180° domain walls due to the magnetic field orientation effect, shows larger magnetostriction coefficient than other samples. The PM coefficient d_{33} ($d_{33} = \mathrm{d}\lambda/\mathrm{d}H$) for Samples 1, 2, and 3 under 1100 Oe is about 30.3, 31.1, and 33.6 nm A^{-1}, respectively. The d_{33} improvement results in a small increase in the nonresonant ME coefficient and significant increase in near resonant frequencies. The mechanical quality factor Q_m of the second peak using the 3 dB frequency bandwidth is further calculated. The Q_m values for Samples 1, 2, and 3 are 23.30, 29.87, and 33.68, respectively. The enhanced Q_m was due to the modified preparation method. The ME coefficient is mainly related to the PM coefficient and can be affected by other factors, such as Young's modulus, demagnetization field, and magnetic permeability. Under the low magnetic field, the measured results can mainly depend

on the demagnetization field. The magnetostrictive properties in this work were measured under quasi-static conditions, which differ from the dynamic measurement results. To sum up, the oriented magnetic field is more effective to improve the magnetostrictive properties than heating in magnetic warm compaction technology.

3b.2.3 Conclusions for Magnetic Warm Compaction

In summary, magnetic warm compaction technology is an effective preparation method of bonded Terfenol-D layered ME composites. The transverse ME voltage coefficient of Terfenol-D/PZT-5H bilayered ME composites is about $6\,V\,cm^{-1}\,Oe^{-1}$, which is three times of that prepared by traditional room temperature pressure molding. The oriented magnetic field contributes more than the heating procedure to enhance the ME voltage coefficient.

3b.3 Multifaceted Magnetoelectric Composites

In this study, ME composite with multifaceted structure is proposed. Specifically, the four-faceted Terfenol-D/Pb(Zr, Ti)O_3, PZT-5H, ME composite consisting of one cubic bonded Terfenol-D composite and four plates of PZT has been fabricated. The ME effect of this kind of composite has been further improved by using the multifaceted structure scheme.

3b.3.1 Experiment for Multifaceted Magnetoelectric Composites

The preparation process is shown in Figure 3b.1. The bonded Terfenol-D was made by using the aforementioned magnetic warm compaction method. Four commercial PZT-5H ceramic plates with $25 \times 10 \times 1\,mm^3$ dimensions were polarized along the thickness direction and bonded with the cubic bonded Terfenol-D composite ($33 \times 10 \times 10\,mm^3$) with glue to form a four-faceted composite. Each PZT plate is electrically isolated from the Terfenol-D composite and other PZT plates. The ME voltage coefficient $\alpha_{E,31}$ was measured by the aforementioned ME measurement system (Figure 3b.6).

3b.3.2 Results and Discussion for Multifaceted Magnetoelectric Composites

The frequency dependence of $\alpha_{E,31}$ with different number of PZT plates in parallel and serial modes was measured under the dc magnetic field of $H_{dc} = 700\,kOe$, as shown in Figures 3b.7 and 3b.8. A strong resonance peak appears at about

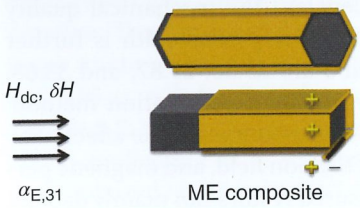

Figure 3b.6 Schematics of bonded Terfenol-D/Pb(Zr, Ti)O_3 ME composites. Zuo *et al.* 2014 [12]. Reproduced with permission of American Institute of Physics.

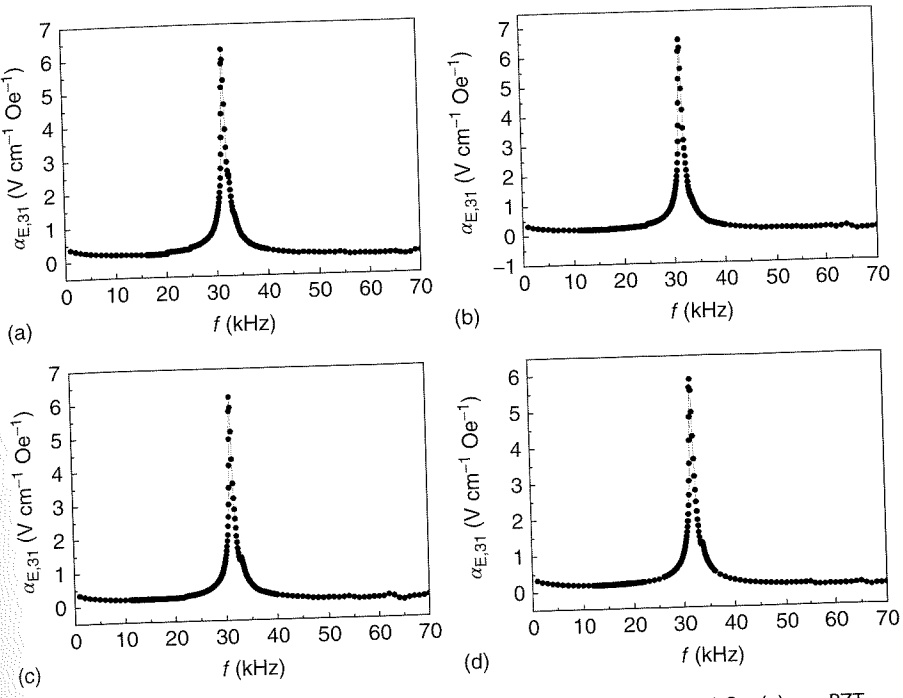

Figure 3b.7 Frequency dependence of $\alpha_{E,31}$ in parallel mode with $H_{dc} = 700$ Oe: (a) one PZT plate; (b) two PZT plates; (c) three PZT plates; and (d) four PZT plates. Zuo *et al.* 2014 [12]. Reproduced with permission of American Institute of Physics.

31.6 kHz in all four cases. As for the parallel mode, the $\alpha_{E,31}$ remains at about 6 V cm^{-1} Oe^{-1} when the number of PZT plates increased from 1 to 4. However, the $\alpha_{E,31}$ increases multiplicatively with the number of PZT plates in the serial mode. The $\alpha_{E,31}$ is improved up to 24 V cm^{-1} Oe^{-1} when four PZT plates were connected in series.

Usually, a piezoelectric resonator is modeled as an LCR oscillator. Given that the four PZT plates are bonded on one single Terfenol-D composite and each PZT plate resonates at the same frequency in this study, the model can be simplified. Only the PZT plates are taken into account when discussing the multiplied ME output voltage. Figure 3b.9 shows the sketch map of parallel and serial modes in this study. Due to the identical properties of the four PZT plates, the total capacitance in parallel and serial modes can be written as

$$C_p = C_1 + C_2 + C_3 + C_4 = 4C_0 \tag{3b.1}$$

$$\frac{1}{C_s} = \frac{1}{C_1} + \frac{1}{C_2} + \frac{1}{C_3} + \frac{1}{C_4} = \frac{4}{C_0} \tag{3b.2}$$

It can be assumed that the four PZT plates are under the same stress state when vibrating under the ac magnetic field if minor differences between each bonding interface are ignored. The piezoelectric effect in PZT arises from the stress-induced charge polarization. Every PZT plate exhibits the same amount of stress-induced charge, which is denoted by Q_0. In parallel mode, the negative

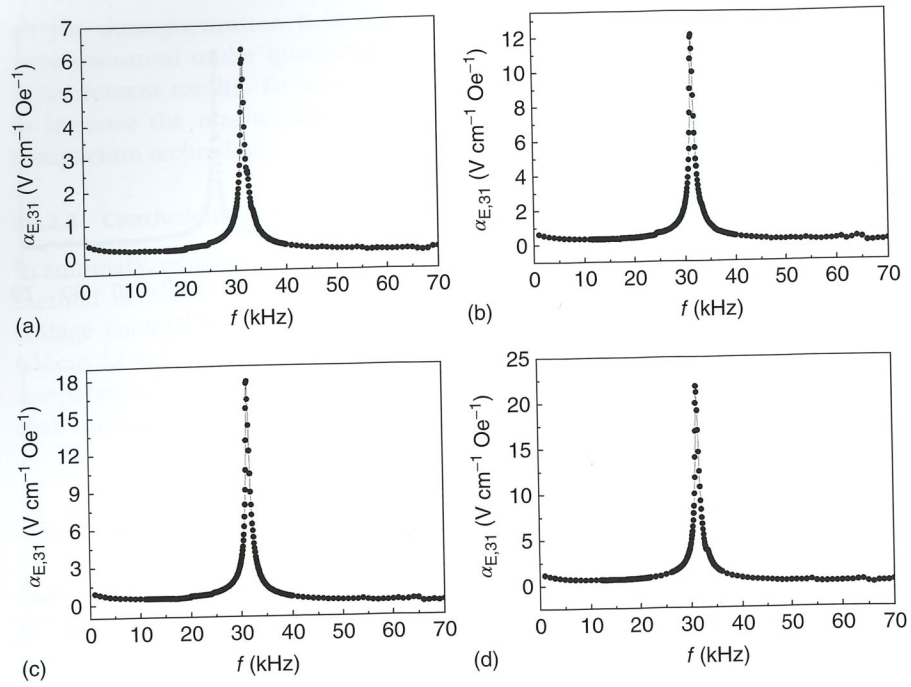

Figure 3b.8 Frequency dependence of $\alpha_{E,31}$ in serial mode with $H_{dc} = 700$ Oe: (a) one PZT plate; (b) two PZT plates; (c) three PZT plates; and (d) four PZT plates. Zuo *et al.* 2014 [12]. Reproduced with permission of American Institute of Physics.

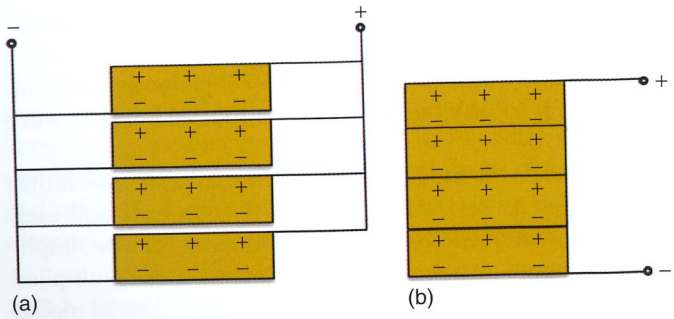

Figure 3b.9 The sketch map of (a) parallel mode and (b) serial mode. Zuo *et al.* 2014 [12]. Reproduced with permission of American Institute of Physics.

and positive charges are accumulated respectively. Thus, the total charge is denoted by $Q_p = 4Q_0$. However, the opposite charges on the two contact surfaces cancel each other out in the circuit for the serial mode. The total charge in the serial mode is denoted by $Q_s = Q_0$. Thus, the ME voltage in the parallel mode is $U_p = Q_p/C_p = U_0$, which indicates that the $\alpha_{E,31}$ remains the same when increasing the number of PZT plates from 1 to 4. The ME voltage in the serial mode is $U_s = Q_s/C_s = 4U_0$. This explains the multiplicative increases of $\alpha_{E,31}$ with the number of PZT plates in the serial mode. Accordingly, the ME

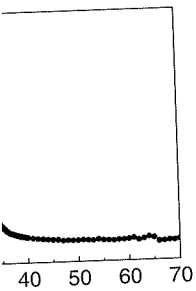

Hz)

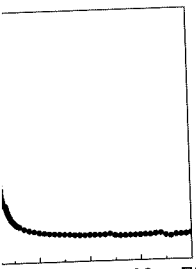

kHz)

0 Oe: (a) one PZT
et al. 2014 [12].

uo *et al.* 2014 [12].

the total charge is
two contact surfaces
The total charge in
ltage in the parallel
remains the same
ne ME voltage in the
plicative increases of
Accordingly, the ME

voltage coefficient will be multiplied in the five-faceted, six-faceted, or other ME composites with this kind of multifaceted structure.

3b.3.3 Conclusions for Multifaceted Magnetoelectric Composites

In conclusion, the ME voltage coefficient is multiplied by employing the multi-faceted structure. The $\alpha_{E,31}$ is improved up to 24 V cm^{-1} Oe^{-1} when four PZT plates were connected in series. This multifaceted structure offers an effective approach to improving ME effect and downsizing the ME devices other than exploiting new material systems.

3b.4 Bonded Cylindrical Composites

Giant ME effect of the ME composites is capable of meeting the demands for practical applications. Typical characteristics of some representative ME composites are given in Table 3b.1. Comparing the advantages and disadvantages, it is valid to consider that substituting Terfenol-D-epoxy (TDE) for Ni to make cylindrical composites can lead to better performance. The aim of this work is to present TDE/PZT cylindrical composites with a simpler one-step room temperature compression molding method that leads to higher magnetoelectric performance and saves processing time, energy, and expenses associated with fabrication due to a simpler and more rapid manufacturing method. The ME voltage coefficient of these cylindrical composites was investigated.

3b.4.1 Experiment for Bonded Cylindrical Composites

The TDE/PZT cylindrical composites were prepared. A detailed schematic of the composites is shown in Figure 3b.10. The PZT cylinder with the

Table 3b.1 Typical characteristics of some representative ME composites.

Representative ME composites	Advantages	Disadvantages	References
Terfenol-D/PZT (2-2-type) laminated composite	Simple and quick fabrication process Large ME voltage coefficient	High eddy current loss at high frequency Brittleness	[11–13]
TDE/PZT (1-3-type) composite	Less eddy current loss Stabile mechanical performance	Complex fabrication process (dice-and-fill procedure) Less effective materials (Terfenol-D ~ 27 vol%) in piezomagnetic phase (TDE)	[13–15]
Ni/PZT cylindrical composite prepared by electrodeposition/electroless-deposition	Preferable structure with larger ME voltage coefficient than 2–2-type laminated composite at same size	Lower magnetoelastic performance of piezoelectric phase (Ni)	[16, 17]

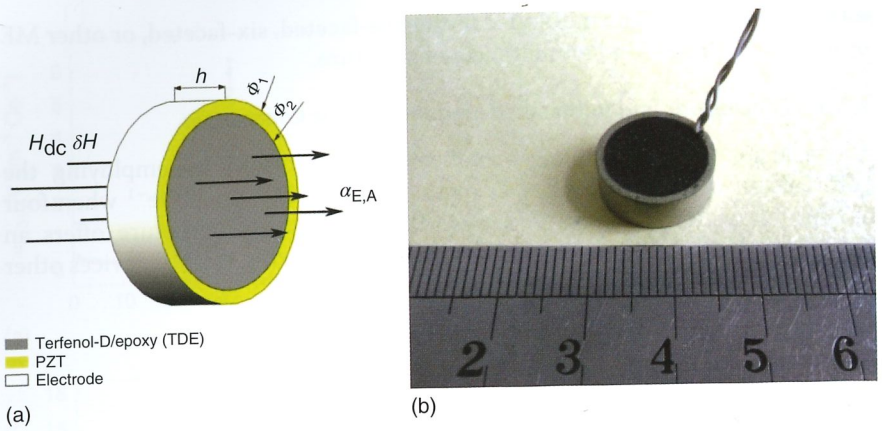

Figure 3b.10 (a) Schematic illustration of the TDE/PZT cylindrical composites. Vectors identify the direction of the applied magnetic field, and the corresponding ME voltage coefficients and (b) picture of the actual sample. The scale is in centimeters. Song *et al.* 2015 http://scitation.aip.org/content/aip/journal/adva/5/3/10.1063/1.4914106. Used under CC BY 3.0 license.

$\Phi_1 \times \Phi_2 \times h = 15 \times 13 \times 5\,\text{mm}^3$ dimensions was polarized along the radial direction with Ni electrodes on both inside and outside surfaces. The Terfenol-D particles with ~180 μm size were obtained by crushing bulk Terfenol-D single crystal in argon. A homogeneous mixture consisting of 12 wt% epoxy resin binder and 88 wt% Terfenol-D particles was compacted by uniaxial pressing with randomly oriented particles. TDE needs 24 h for curing. The TDE with randomly oriented Terfenol-D particles is cured without prestress. The ME effect of the TDE/PZT composites was obtained using the aforementioned ME measurement system. The ME voltage coefficient, $\alpha_{E,A}$, was measured when H_{dc} and δH were applied along the axial direction of the cylinder.

3b.4.2 Results and Discussion for Bonded Cylindrical Composites

Figure 3b.11 shows typical $\alpha_{E,A}$ and H_{dc} dependence on frequency for the Terfenol-D/PZT composites. As seen in Figure 3b.11a, a giant ME coefficient $\alpha_{E,A}$ of $3.37\,\text{V cm}^{-1}\,\text{Oe}^{-1}$ at 64.8 kHz is observed. This giant ME response at high frequency is attributed to the electromechanical resonance [19], which significantly enhances the elastic coupling interaction between the TDE medium and the PZT cylinder. The ME coefficient $\alpha_{E,A}$ dependence on the magnetic field is shown in Figure 3b.11b. At low magnetic field, $\alpha_{E,A}$ increases approximately linearly with the magnetic bias due to the increasing magnetostriction, while at high magnetic field, $\alpha_{E,A}$ increases to a maximum value at the optimal magnetic field, $H_m = 2.6$ kOe, and then, $\alpha_{E,A}$ decreases. The maximum ME voltage coefficient of these composites, $\alpha_{E,A}$, is $3.35\,\text{V cm}^{-1}\,\text{Oe}^{-1}$.

According to the Pan's model [17], cylindrical ME composite axial coupling mode can be dealt with as an effective plate bilayered ME composite in the width direction mode. The dimensions of the simplified plate bilayered ME composites are $h \times L^{\text{eff}} \times t$, where t is the total thickness of the piezoelectric phase, t_{PE}, and the PM phase, t_{PM}, as shown in Figure 3b.12. To ensure similar conditions of

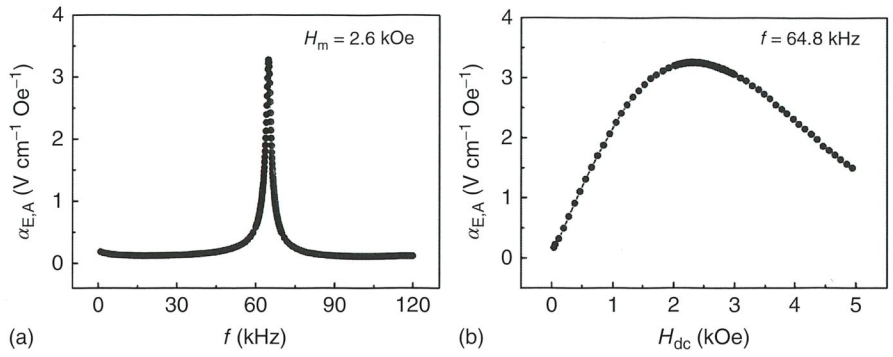

Figure 3b.11 (a) $\alpha_{E,A}$ dependence on the ac magnetic field frequency (f) at the optimal magnetic field (H_m), corresponding to the maximum ME coupling and (b) $\alpha_{E,A}$ dependence on H_{dc} at the resonant frequency. Song *et al.* 2015 http://scitation.aip.org/content/aip/journal/adva/5/3/10.1063/1.4914106. Used under CC BY 3.0 license.

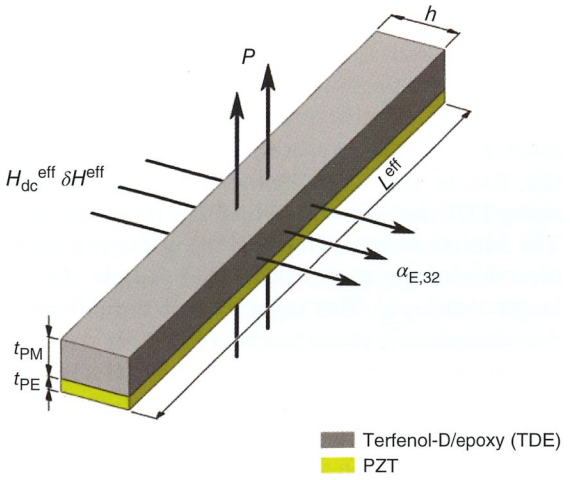

Figure 3b.12 Schematic illustration of the TDE/PZT planar laminated composites for the differential coefficient calculation. Song *et al.* 2015 http://scitation.aip.org/content/aip/journal/adva/5/3/10.1063/1.4914106. Used under CC BY 3.0 license.

the ME coupling, this study designated $t_{PE} = 1$ mm, $h = 5$ mm (the same as the PZT cylinder) with the effective length of about 41 mm ($L^{eff} = \pi \cdot \Phi_2$). To have the same contact area between the two phases, t_{PM} was set at about 3 mm ($\pi \cdot r^2 = t_{PM} \cdot h$), which guaranteed that there is the same TDE volume. So that $h \times L^{eff} \times t = h \times L^{eff} \times (t_{PE} + t_{PM}) = 5\,\text{mm} \times 41\,\text{mm} \times 4\,\text{mm}$. After simplification, the effective magnetic fields H_{dc}^{eff} and δH^{eff} are along the width direction, and their values are the same as the measured and the applied magnetic fields ($H_{dc}^{eff} = H_{dc}$, $\delta H^{eff} = \delta H$).

The effective plate bilayered ME composite sample has been prepared. Figure 3b.13 shows the test results of the effective plate sample. The ME voltage coefficient $\alpha_{E,A}$ is in a transverse direction of the plate composite, while $\alpha_{E,32}$ is about 2.75 V cm^{-1} Oe^{-1} at the corresponding 1.7 kOe optimal magnetic field and 31 kHz resonant frequency. Comparing the two composites, the peak value of $\alpha_{E,A}$ is 3.37 V cm^{-1} Oe^{-1}, about 1.2 times larger than $\alpha_{E,32}$. This demonstrates

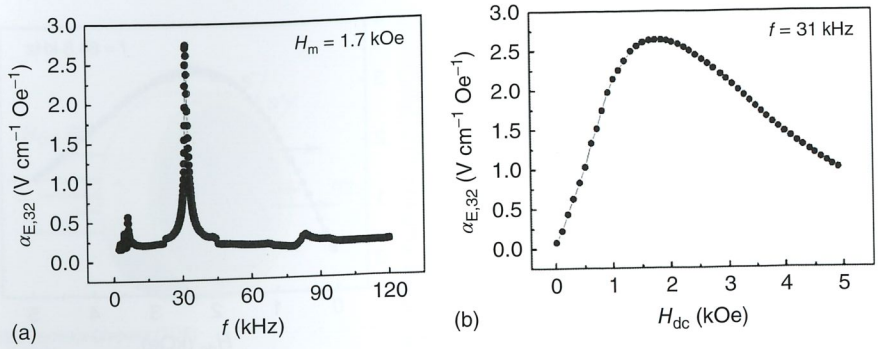

Figure 3b.13 (a) $\alpha_{E,32}$ dependence on the ac magnetic field frequency (f) at the optimal magnetic field (H_m), corresponding to the maximum ME coupling and (b) $\alpha_{E,32}$ dependence on H_{dc} of at the resonant frequency. Song *et al.* 2015 http://scitation.aip.org/content/aip/journal/adva/5/3/10.1063/1.4914106. Used under CC BY 3.0 license.

that the self-bound state of the cylindrical structure can promote the ME effect, compared with the planar laminated structure with more free surfaces [17, 20]. There is a slight difference in H_m between the two samples with the same PM phases, suggesting that H_m strongly depends on the geometry of the composites.

The complex structure (such as the cylindrical structure) of the ME composites is usually prepared by Ni electrodeposition or electroless deposition [16, 21]. In this work, cylindrical ME composites were successfully obtained using TDE instead of Ni, which has much better magnetostrictive performance. The ME effect was compared using the representative axial mode with the 32 direction of the planar laminated sample. The overall $\alpha_{E,A}$ is about 1.2 times larger than $\alpha_{E,32}$. This suggests that the different bonding layered structure of the piezoelectric phase (such as PZT) has a different stress state. The cylindrical PE phase is under higher normal stress and lower shear stress due to the self-bound state. By contrast, the planar PE phase is primarily under shear stress due to the planar laminated structure, which allows more free surfaces. Since the cylinder can be simplified as a bilayer plate, $\alpha_{E,A}$ and $\alpha_{E,32}$ are equivalent for the ME composite with the $5 \times 41 \times 4\,mm^3$ dimensions. Using the Pan's model conversion [17], the dimensions of the ME composites can be decreased further using the TDE/PZT cylindrical composites with the same ME voltage coefficient.

3b.4.3 Conclusions for Bonded Cylindrical Composites

The TDE/PZT cylindrical ME composites have been prepared using the one-step compression molding, without any additional processes. The fabrication process is much simpler than the previous bonded TDE/PZT composites, which makes it more cost efficient. The experimental results have demonstrated that this composite structure has larger ME voltage coefficient and smaller geometric dimensions compared with the effective planar laminated composites due to the self-bound state. The favorable performance of the TDE/PZT cylindrical composites with a simple and effective manufacturing method can facilitate the ME devices miniaturization and design for practical applications.

3b.5 Multi-electrode Cylinder Composites

Creating an optimized structural design to utilize PM materials in an efficient way, namely by enhancing the magnetoelectric efficiency factors, would allow PM materials to contribute more power (ME effect) per unit weight [22]. Therefore, it would be more beneficial to create more efficient lightweight devices for reducing the cost of devices and applications. In order to attain both high ME effect and less PM material usage, multi-electrode cylinder layered ME composites PZT/Terfenol-D/PZT (P-T-P), based on the advantages of serial mode laminated Terfenol-D/PZT composites and cylinder layered Ni/PZT composites, were prepared by compression molding with epoxy [12, 16]. Furthermore, a basic structural monocyclic Terfenol-D/PZT (T-P) composite with a single electrode layer and a Terfenol-D/PZT/Terfenol-D/PZT (T-P-T-P) composite with the same overall dimensions (same two layers of electrode PZT structures but more Terfenol-D usage than the P-T-P) were prepared for comparison. The vertical mode voltage coefficients ($\alpha_{E,V}$) of the samples were investigated.

3b.5.1 Experiment for Multi-electrode Cylinder Composites

The proposed layered ME composites, as shown in Figure 3b.14, were made up of a positive magnetostrictive phase Terfenol-D and piezoelectric PZT phase. The PZT cylinders were polarized along the radial direction after electroplating a thin layer of Ni on the inside and outside surfaces. Terfenol-D was made by the aforementioned TDE method. The ME effect of the Terfenol-D/PZT composites was obtained using the aforementioned ME measurement system as well. The vertical mode ME voltage coefficient, $\alpha_{E,V}$, was measured when H_{dc} and δH were applied along the vertical direction of the cylinder in Figure 3b.15a. For comparison, the T-P, P-T-P, and T-P-T-P cylindrical layered composites were prepared. Both P-T-P and T-P-T-P have two layers of PZT connected in series [12] (inner and outer PZT electrodes connected in series). The geometrical arrangements and components of three composite samples are shown schematically in Figure 3b.14.

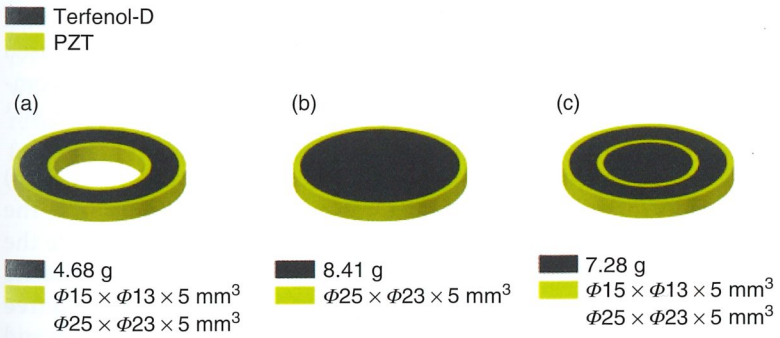

Figure 3b.14 Schematics illustrating the geometrical arrangement of Terfenol-D/PZT cylindrical ME composites: (a) P-T-P; (b) T-P; and (c) T-P-T-P. Song *et al.* 2016 [23]. Reproduced with permission of Elsevier.

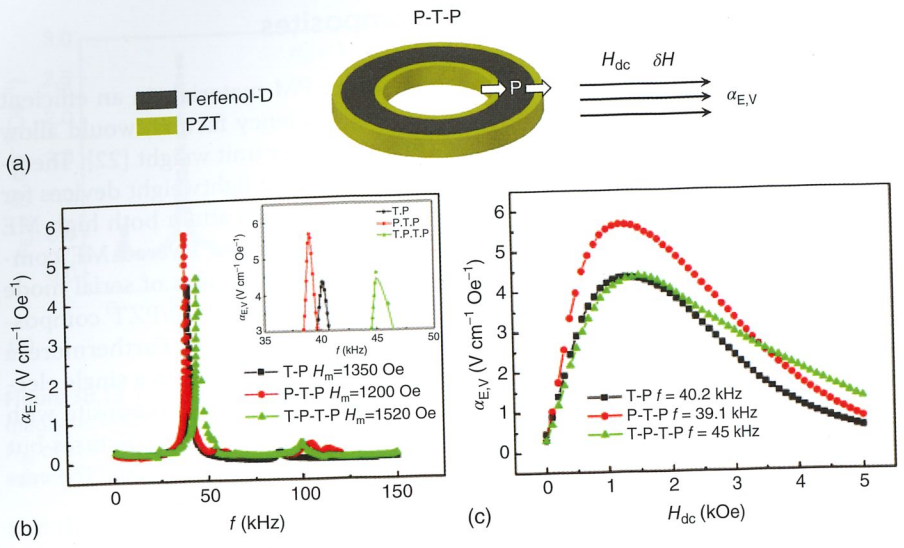

Figure 3b.15 (a) Schematic of the composite mode (the directions of applied magnetic field and polarization) (showing P-T-P as an example); (b) the $\alpha_{E,V}$ dependence on the ac magnetic field frequency (f) at the optimal magnetic field (H_m) of the three samples, corresponding to the maximum ME coupling; and (c) the H_{dc} dependence of $a_{E,A}$ at the resonance frequency. Song *et al.* 2016 [23]. Reproduced with permission of Elsevier.

3b.5.2 Results and Discussion for Multi-electrode Cylinder Composites

Figure 3b.15a illustrates the directions of the applied magnetic field and polarization of the composite in the vertical mode (P-T-P is shown as an example). Figure 3b.15b shows the ME voltage coefficient, $\alpha_{E,V}$, dependency on frequency in the vertical mode for the three Terfenol-D/PZT cylinder layered composites at the respective optimal magnetic field (H_m). As shown in Figure 3b.15b, each composite has one main resonance peak of $a_{E,V}$, each having relatively close resonant frequencies. The slight difference in the three resonant frequencies is related to the electromechanical resonance of the three samples with relatively different structures and mass [24]. Figure 3b.15c shows the H bias (H_{dc}) dependence of the ME coefficient ($a_{E,V}$) at the respective resonant frequency. The $\alpha_{E,V}$ increased with H_{dc} until the local maximum value was reached for the three tested composites. By comparison, the P-T-P composite had higher $a_{E,V}$ of 5.8 V cm^{-1} Oe^{-1} compared to that of the other two composites T-P and T-P-T-P.

Figure 3b.16 shows a schematic illustration of the contact surfaces (cyan area) and the free surfaces (dark gray area) of the three composites without PZT. The contact surface is defined as the contact area of Terfenol-D and PZT, while the other areas are the free surfaces [20]. As shown in Figure 3b.16, each composite has different contact and free areas. The total area of contact surfaces and free surfaces of each composite was calculated using the circle area ($A_{circle} = \pi \cdot r^2$) and the cylinder area ($A_{cylinder} = \pi \cdot D \times t$), where A is the area, r is the radius, D is the diameter, and t is the thickness of the composite. An effective working surface specific value (A_{eff}) is calculated by dividing the area of contact surface by the

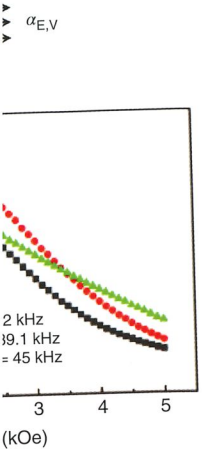

lied magnetic field
on the ac magnetic
, corresponding to
nance frequency.

posites

ic field and polar-
n as an example).
ency on frequency
ayered composites
igure 3b.15b, each
latively close reso-
quencies is related
relatively different
$_{dc}$) dependence of
The $\alpha_{E,V}$ increased
three tested com-
of 5.8 V cm^{-1} Oe^{-1}
'-P.
urfaces (cyan area)
s without PZT. The
and PZT, while the
16, each composite
ct surfaces and free
a ($A_{circle} = \pi \cdot r^2$) and
the radius, D is the
ive working surface
ntact surface by the

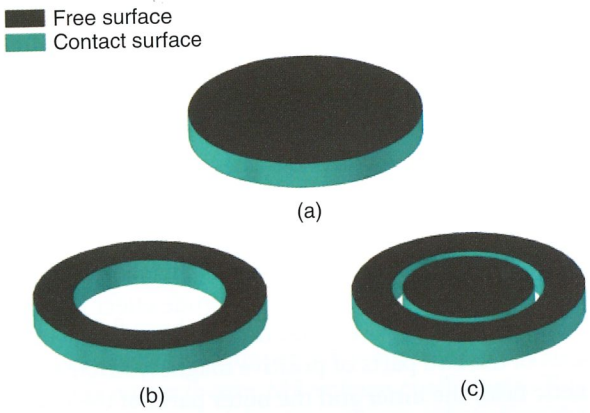

Figure 3b.16 Schematics illustrating the contact surfaces and the free surfaces of the composites (without PZT): (a) P-T-P; (b) T-P; and (c) T-P-T-P. Song *et al.* 2016 [23]. Reproduced with permission of Elsevier.

area of the free surface for each composite. In comparison, the P-T-P has the largest A_{eff} value of 1.25, whereas T-P A_{eff} is equal to 0.43 and T-P-T-P A_{eff} is equal to 1.08.

According to the Pan's differential coefficient model [17], a vertical coupling mode cylindrical composite can be simplified as an effective 2–2 laminated ME composite. In the vertical mode, both $\alpha_{E,31}$ and $\alpha_{E,33}$ of this effective ME composite contribute to the ME effect ($a_{E,V}$) at the same time [17]. Based on the constitutive equation [13], when a perfect interface between the PM and PE phases occurs in an ideal case, and magnetic field is applied along the transverse or longitudinal direction of the laminated ME composite, the constitutive equation can be directly solved by an averaging method to estimate effective material parameters. The transverse ME coefficient is given as

$$\alpha_{E,31} = \frac{E_3}{H_1} = \frac{-f(1-f)(q_{11}+q_{21})d_{31}}{{}^{p}\varepsilon_{33}\bar{s} - 2fd_{31}^2} \tag{3b.3}$$

The longitudinal ME coefficient is given as

$$\alpha_{E,33} = \frac{E_3}{H_3} = \frac{2f(1-f)d_{31}q_{31}\mu_0\bar{s}}{(2fd_{31}^2 - {}^{p}\varepsilon_{33}\bar{s})[\bar{\mu}\bar{s} + 2q_{31}^2(1-f)^2]} \tag{3b.4}$$

Here, q is the PM coupling coefficient, d is the piezoelectric coupling coefficient, ε is the dielectric constant, and $\bar{s}$ is the effective compliance. $\bar{\mu} = f\mu_0 + (1-f)^m\mu_{33}$, where μ_0 and μ_{33} are permeability of the free space and the magnetic phase, respectively. Superscript p denotes the piezoelectric phase. Here, f is the volume fraction of the magnetic phase:

$$f = \frac{v_{\text{Terfenol-D}}}{v_{\text{Terfenol-D}} + v_{\text{PZT}}} \tag{3b.5}$$

where v is the volume of the PE and PM phases. The T-P, P-T-P, and T-P-T-P samples all have the same material parameters, except for the volume fraction of the magnetic phase. The volume fractions of the three samples are $f_{\text{T-P}} = 0.85$, $f_{\text{P-T-P}} = 0.66$, and $f_{\text{T-P-T-P}} = 0.76$, respectively, based on Eq. (3b.5). The calculation results demonstrated that the P-T-P composite has higher $a_{E,V}$, which is attributed to an optimal volume fraction (f) of the PM phase, according to the

analogous computation results (optimal $f \sim 0.6$) [25]. Additionally, a larger A_{eff} can create more efficient interfacial strain coupling between the PM and the PE phases with same volume fraction [26]. When f is constant, the following equation can be used:

$$\alpha_E \propto A_{eff} \tag{3b.6}$$

The P-T-P composite, which had an optimal volume fraction and the largest A_{eff}, yielded the highest ME voltage coefficient of the three composite samples.

Additionally, the ME voltage coefficient of the P-T-P composite can also be enhanced by the series multi-electrode effect [12]. While the P-T-P and T-P-T-P composites both have series multi-electrode effect, the T-P-T-P composite consists of the two parts of positive magnetostrictive Terfenol-D phase. In the magnetic field, the inner and the outer parts of the magnetostrictive phases produce normal stress at the same time along the radical direction, from the center of the circle to PZT, inducing PZT dielectric polarization, thus producing the ME effect [17]. In the series mode, the inner and the outer PZT layers contribute to the ME voltage coefficient together [12]. However, for the inner PZT layer of the T-P-T-P composite, normal stress works on both inner and outer surfaces following along the same direction weakening the polarization [17]. Hence, it weakens the overall ME effect of the T-P-T-P composite.

The measurements of the ME efficiency factor (ME-EF) were conducted. The ME-EF is defined as the α_E contribution of the unit weight PM material, using $\text{ME-EF} = \alpha_{E,V}/m_{\text{Terfenol-D}}$. For the P-T-P composite, $5.8\,\text{V cm}^{-1}\,\text{Oe}^{-1}$ is divided by 4.68 g, resulting in the ME-EF of $1.24\,\text{V cm}^{-1}\,\text{Oe}^{-1}\,\text{g}^{-1}$. It is the highest in the three composites, even higher than the composite with excellent $\alpha_E = 24\,\text{V cm}^{-1}\text{Oe}^{-1}$ ($\text{ME-EF} = 0.92\,\text{V cm}^{-1}\text{Oe}^{-1}\,\text{g}^{-1}$), which consists of 26 g Terfenol-D and four PZT parts connected in series. The $\alpha_{E,V}$, ME-EF, and A_{eff} of each sample are listed in Table 3b.2.

The outstanding ME-EF of T-P-T cylinder composite represents the T-P-T mode of the ME composite with more efficient utilization of the PM material. It is a result of A_{eff} of the PM and PE phases, boundary and stress conditions of the PM and PE layers and the series multi-electrode effect [12, 20]. Hence, the P-T-P composites have outstanding advantages of both high ME voltage coefficients and less usage of the PM material, compared with the T-P and the T-P-T-P composites. The P-T-P layered configuration is just an elementary designed structure, not an optimal design. This study provides a way for efficient utilization of PM materials for the ME composites. Similar, but even better structural designs can

Table 3b.2 ME voltage coefficients ($\alpha_{E,V}$), ME efficiency factor (ME-EF), and effective working surface specific value (A_{eff}) of the three samples.

Sample	$\alpha_{E,V}$ ($\text{V cm}^{-1}\,\text{Oe}^{-1}$)	ME-EF ($\text{V cm}^{-1}\,\text{Oe}^{-1}\,\text{g}^{-1}$)	s_{eff} (Contact/free)
T-P	4.4	0.52	0.43
P-T-P	5.8	1.24	1.25
T-P-T-P	4.6	0.63	1.08

widely benefit from cost efficiency and result in lighter magnetic sensors, magnetometers, transducers, and stray capacitor devices [27–29].

3b.5.3 Conclusions for Multi-electrode Cylinder Composites

In summary, the study investigated the ME voltage coefficients of the mono/multi-electrode cylinder layered Terfenol-D/PZT ME composites with three different structures for enhancing ME efficiency. The ME voltage coefficient, $\alpha_{E,V}$, of the P-T-P mode composite is 5.8 V cm^{-1} Oe^{-1} at the resonant frequency, and the ME-EF is 1.24 V cm^{-1} Oe^{-1} g^{-1}, which is more than two times higher than the T-P and the T-P-T-P modes. The results of the study demonstrate that this type of hollow multi-electrode cylinder ME composite uses lower amounts of PM materials but yields higher/better ME voltage coefficients. This finding indicates that creating similar structural designs will not only reduce the weight but also the cost to manufacture ME devices for practical applications, such as magnetic sensors, earth-magnetism navigation, mineral exploration, transducers, and magnetometers.

3b.6 Polymer Content and Particle Size Effects

In an effort to optimize the polymer-bonded ME composites, polymer-bonded TDE/PZT cylinder ME composites with varying polymer content and particle size have been investigated. The axial mode voltage coefficient ($\alpha_{E,A}$) of the samples was examined.

3b.6.1 Experiment for Polymer Content and Particle Size Effects

The Terfenol-D particles were obtained by crushing bulk Terfenol-D single-crystal alloy in argon atmosphere. The XRD pattern of the particles is shown in Figure 3b.17a. The proposed Terfenol-D/PZT cylindrical ME composites were made up of the aforementioned Terfenol-D particles and the PZT cylinder. The PZT cylinder was polarized along the radial direction. The Terfenol-D particles were compacted by uniaxial compression in the PZT cylinder, fabricated at 2 MPa pressure. The TDE needed 24 h for curing. A detailed preparation method and schematic of the Terfenol-D/PZT cylindrical composite are shown elsewhere [18]. The ME performance of the Terfenol-D/PZT composites was obtained using the aforementioned ME measurement system. The axial mode ME voltage coefficient, $\alpha_{E,A}$, was measured when H_{dc} and δH were applied along the axial direction of the cylinder.

3b.6.2 Results and Discussion for Polymer Content and Particle Size Effects

The microstructure of crushed Terfenol-D particles after sieving was examined by X-ray diffraction. The XRD pattern in Figure 3b.17a of the particles is almost identical to the standard Terfenol-D XRD pattern, meaning that the crystal phase was not changed during the fabrication process [31]. The Terfenol-D particles with four different size ranges (<75, 75–100, 100–150, and 150–180 μm) were

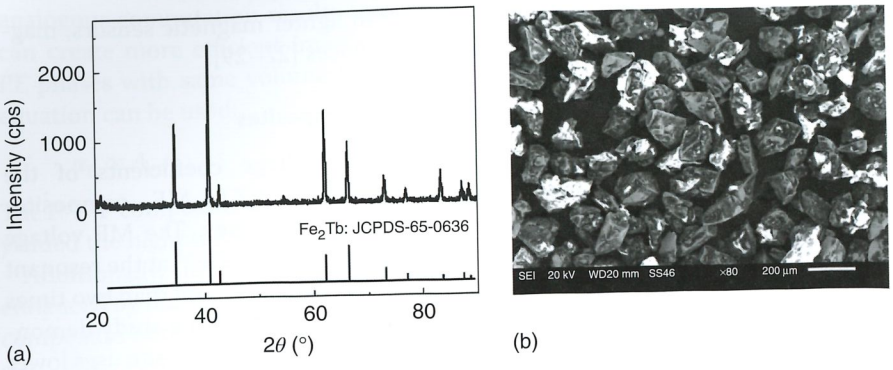

Figure 3b.17 (a) XRD pattern of the crushed Terfenol-D particles and (b) Terfenol-D particles with the 150–180 µm size, observed by SEM. Song *et al.* 2016 [30]. Reproduced with permission of Elsevier.

obtained using a set of two sieves with different meshes. Hence, the <75 µm range indicates the particles that passed through the sieve with an opening size of 75 µm. The 75–100 µm range indicates that the particles passed through a 100 µm opening sieve but were blocked by the 75 µm sieve. The particle size distribution is ideally uniform after sieving, noted by Figure 3b.17b, for the 150–180 µm particle size range.

The epoxy content of the composites was studied with five different weight ratios of 9, 12, 14, 16, and 19 wt%. Figure 3b.18 shows the ME voltage coefficient, $\alpha_{E,A}$, dependency on the volume ratio of various epoxy content with the 150–180 µm Terfenol-D particle size. As seen in Figure 3b.18, the ME voltage

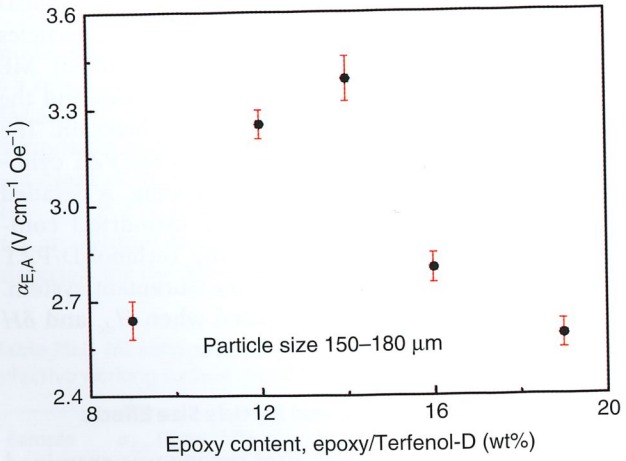

Figure 3b.18 The ME voltage coefficient, $\alpha_{E,A}$, dependence on the volume ratio of epoxy content. The results are for the sample with the particle size of 150–180 µm. Song *et al.* 2016 [30]. Reproduced with permission of Elsevier.

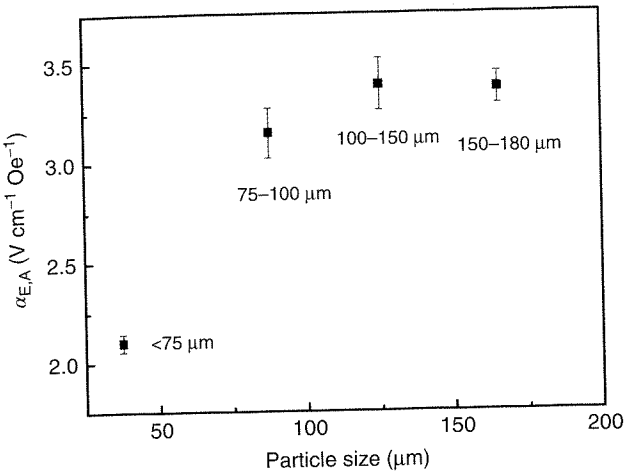

Figure 3b.19 The ME voltage coefficient, $\alpha_{E,A}$, dependence on the Terfenol-D particle size. The results are for the samples fabricated with the epoxy content of 0.14 wt%. Song *et al.* 2016 [30]. Reproduced with permission of Elsevier.

coefficient is greatly affected by the epoxy content. The ME voltage coefficient reached the maximum value of $\alpha_{E,A} = 3.37\ \text{V cm}^{-1}\ \text{Oe}^{-1}$ when the epoxy content was 14 wt%. The ME voltage coefficient was degraded when the epoxy content was below 14 wt%. This could be due to the epoxy's inability to effectively play the binder and the lubricant roles at lower epoxy content [32]. When epoxy content increased over 14 wt%, the ME performance decreased rapidly due to the dilution effect by the nonfunctional polymer phase [33].

Figure 3b.19 shows the ME voltage coefficient, $\alpha_{E,A}$, particle size dependency for different Terfenol-D particle ranges of <75, 75–100, 100–150, and 150–180 μm, with an epoxy content of 0.14 wt%. As seen in Figure 3b.19, the ME voltage coefficient of the <75 μm particle size, $\alpha_{E,A} = 2.1\ \text{V cm}^{-1}\ \text{Oe}^{-1}$, is much lower than others. When the particle size is between 100 and 150 μm, the ME voltage coefficient is the highest, up to $3.4\ \text{V cm}^{-1}\ \text{Oe}^{-1}$. This result demonstrated that the ME voltage coefficient was also degraded when Terfenol-D particles were small. When particle size is between 100 and 180 μm, the composite can get roughly 1.6 times higher ME performance, compared with the particle size less than 75 μm.

3b.6.3 Conclusions for Polymer Content and Particle Size Effects

In summary, the axial ME voltage coefficient of the polymer-bonded cylindrical Terfenol-D/PZT ME composites was studied. The voltage coefficient can be distinctly influenced by both polymer content and particle size. The composite with an epoxy content of 0.14 wt% and 100–150 μm particle sizes exhibited better overall ME performance. These findings promote selecting the appropriate polymer content and particle size to optimize the fabrication of the polymer-bonded ME composites for high ME performance to meet practical applications.

Acknowledgments

This work was supported by the National Natural Science Foundation of China (U1360202, 51472030, and 51502014), by the Beijing Nova program (Z141103001814006), by the Fundamental Research Funds for the Central Universities (Project No.: FRF-TP-14-001C1), and the China Postdoctoral Science Foundation Funded Project (Project No.: 2014M560885). Alex Volinsky acknowledges the support from the National Science Foundation under the IRES 1358088 grant. Yang Song acknowledges the support from the China Scholarship Council (CSC No.: 201506460047).

References

1 Eerenstein, W., Mathur, N.D., and Scott, J.F. (2006) *Nature*, **442**, 759.
2 Bibes, M. and Barthelemy, A. (2008) *Nat. Mater.*, **7**, 425.
3 Hu, J.M., Chen, L.Q., and Nan, C.W. (2016) *Adv. Mater.*, **28**, 15.
4 Yang, H., Zhang, G., Lin, Y., and Wang, F. (2015) *Mater. Lett.*, **157**, 99.
5 Lee, J.H., Fang, L., Vlahos, E., Ke, X., Jung, Y.W., Kourkoutis, L.F., Kim, J., Ryan, P.J., Heeg, T., Roeckerath, M., Goian, V., Bernhagen, M., Uecker, R., Hammel, P.C., Rabe, K.M., Kamba, S., Schubert, J., Freeland, J.W., Muller, D.A., Fennie, C.J., Schiffer, P., Gopalan, V., Johnston-Halperin, E., and Schlom, D.G. (2010) *Nature*, **466**, 954.
6 Shi, Z., Tong, Y., Deng, S., Xue, H., Yang, S., Lu, Y., Wang, C., and Liu, X. (2013) *Appl. Phys. Lett.*, **103**, 032903.
7 Liu, B., Fang, Y., Han, Z., Yan, S., Zhou, W., Qian, B., Wang, D., and Du, Y. (2016) *Mater. Lett.*, **164**, 425.
8 Lu, M., Mei, L., Jeong, D., Xiang, J., Xie, H., and Zhang, Q. (2015) *Appl. Phys. Lett.*, **106**, 112905.
9 Lim, S., Kim, S., Kang, S., Park, J., Nam, J., and Son, D. (1999) *J. Magn. Magn. Mater.*, **191**, 113.
10 Martins, P. and Lanceros-Méndez, S. (2013) *Adv. Funct. Mater.*, **23**, 3371.
11 Zuo, Z.J., Pan, D., Jia, Y.M., Tian, J.J., Zhang, S.G., and Qiao, L.J. (2014) *J. Alloys Compd.*, **587**, 287.
12 Zuo, Z.J., Pan, D., Lu, J., Zhang, S.G., Tian, J.J., Qiao, L.J., and Volinsky, A.A. (2014) *Appl. Phys. Lett.*, **104**, 032906.
13 Nan, C.W., Bichurin, M.I., Dong, S.X., Viehland, D., and Srinivasan, G. (2008) *J. Appl. Phys.*, **103**, 031101.
14 Ma, J., Shi, Z., and Nan, C.W. (2007) *Adv. Mater.*, **19**, 2571.
15 Ma, J., Hu, J., Li, Z., and Nan, C.W. (2011) *Adv. Mater.*, **23**, 1062.
16 Pan, D., Wang, J., Zuo, Z., Zhang, S., Qiao, L., and Volinsky, A.A. (2014) *Appl. Phys. Lett.*, **104**, 122903.
17 Pan, D., Zhang, S.G., Volinsky, A.A., and Qiao, L.J. (2008) *J. Phys. D: Appl. Phys.*, **41**, 205008.
18 Song, Y., Pan, D., Wang, J., Zuo, Z., Zhang, S., Liu, B., and Volinsky, A.A. (2015) *AIP Adv.*, **5**, 037104.

19 Bichurin, M., Filippov, D., Petrov, V., Laletsin, V., Paddubnaya, N., and Srinivasan, G. (2003) *Phys. Rev. B*, **68**, 1324081.
20 Pan, D., Tian, J.J., Zhang, S.G., Sun, J.S., Volinsky, A.A., and Qiao, L.J. (2009) *Mater. Sci. Eng., B*, **163**, 114.
21 Xie, D., Wang, Y.G., and Cheng, J.H. (2014) *J. Alloys Compd.*, **615**, 298.
22 Ma, F.D., Jin, Y.M., Wang, Y.U., Kampe, S.L., and Dong, S.X. (2014) *Acta Mater.*, **70**, 45.
23 Song, Y., Pan, D., Xu, L., Liu, B., Volinsky, A.A., and Zhang, S. (2016) *Mater. Des.*, **90**, 753.
24 Pan, D.A., Wang, J., Zuo, Z., Zhang, S., Liu, B., Volinsky, A.A., and Qiao, L. (2014) *Mater. Lett.*, **133**, 255.
25 Wu, G., Zhang, R., Zhang, L., Zhu, H., and Zhang, N. (2013) *J. Appl. Phys.*, **113**, 214105.
26 Pan, E. and Wang, R. (2009) *J. Phys. D: Appl. Phys.*, **42**, 245503.
27 Dong, S.X., Zhai, J.Y., Li, J.F., and Viehland, D. (2006) *Appl. Phys. Lett.*, **89**, 252904.
28 Jia, Y., Xue, A.X., Zhou, Z., Wu, Z., Chen, J., Ma, K., Zhang, Y., Zhou, J., Wang, Y., and Chan, H.L.W. (2013) *Int. J. Hydrogen Energy*, **38**, 14915.
29 Liu, Y., Jiao, J., Li, L., Di, W., Zhao, X., Luo, H., and Li, X. (2014) *Sens. Actuators, A*, **211**, 15.
30 Song, Y., Liu, B., Pan, D., Xu, L., Volinsky, A.A., and Zhang, S. (2016) *Mater. Lett.*, **175**, 93.
31 Liu, M., Li, S., Zhou, Z., Beguhn, S., Lou, J., Xu, F., Lu, T.J., and Sun, N.X. (2012) *J. Appl. Phys.*, **112**, 063917.
32 Kadiyala, A.K. and Bijwe, J. (2013) *Wear*, **301**, 802.
33 Liu, J., Pan, Z., Song, X., Zhang, Z., and Ren, W. (2015) *J. Appl. Phys.*, **117**, 17A914.

WILEY-VCH

The first book on this topic provides a comprehensive and well-structured overview of the fundamentals, synthesis and emerging applications of magnetoelectric polymer materials.

Following an introduction to the basic aspects of polymer based magnetoelectric materials and recent developments, subsequent chapters discuss the various types as well as their synthesis and characterization. There then follows a review of the latest applications, such as memories, sensors and actuators. The book concludes with a look at future technological advances.

An essential reference for entrants to the field as well as for experienced researchers.

Senentxu Lanceros-Méndez *graduated in physics at the University of the Basque Country, Leioa, Spain. He obtained his PhD degree at the Institute of Physics of the Julius-Maximilians-Universität Würzburg, Germany. He was a Research Scholar at Montana State University, Bozeman, MT, USA and visiting scientist at the Pennsylvania State University, USA and University of Potsdam, among others. Since 2016 he is a Ikerbasque Professor at the BCMaterials, Basque Center for Materials, Applications and Nanostructures, Derio, Spain. He is an Associate Professor at the Physics Department of the University of Minho, Portugal (on leave), where he belongs to the Center of Physics. From 2012 to 2014 he was also an Associate Researcher at the INL – International Iberian Nanotechnology Laboratory. His work is focused in the area of smart materials for sensors and actuators, energy and biomedical applications.*

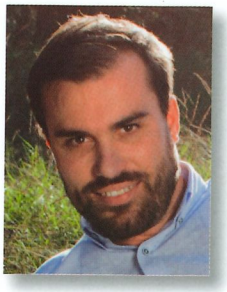

Pedro Martins *graduated in Physics and Chemistry in 2006 and received the PhD degree in Physics in 2012, both from the University of Minho, Braga, Portugal. From 2012 to 2014 he was also a Visiting Researcher at the INL – International Iberian Nanotechnology Laboratory. He is now a postdoctoral researcher in the University of Minho, Braga, Portugal and his work is focused on polymer-based magnetoelectric materials and electroactive polymers for advanced technological applications. He collaborates with the Basque Country University, Spain; Wollongong University, Australia and Cambridge University, United Kingdom, among others.*

ISBN 978-3-527-34127-6

www.wiley-vch.de